

# Multi-Head Spatial Atomic Layer Deposition: A Robust Approach for Precise Doping and Nanolaminate Fabrication in Open-Air Environments

Hayri Okcu<sup>\*,†,‡</sup>, Martin Ignacio Broens<sup>†</sup>, Vijaya Shanthi Paul Raj<sup>†</sup>, Pia Javiera Vasquez Rivera<sup>†</sup>, Gustavo Ardila<sup>‡</sup> and David Muñoz-Rojas<sup>\*,†</sup>

<sup>†</sup>*Univ. Grenoble Alpes, CNRS, Grenoble INP, LMGP, 38000 Grenoble, France*

<sup>‡</sup>*Univ. Grenoble Alpes, Univ. Savoie Mont Blanc, CNRS, Grenoble INP, CROMA, 38000 Grenoble, France*

E-mail: [hayri.okcu@grenoble-inp.fr](mailto:hayri.okcu@grenoble-inp.fr), [david.munoz-rojas@grenoble-inp.fr](mailto:david.munoz-rojas@grenoble-inp.fr)

## Supplementary Information

### Computational Fluid Dynamics (CFD) simulation

A fine, physics-controlled mesh (minimum elemental quality: 0.07846) was employed in COMSOL<sup>®</sup> to capture spatial thickness gradients, particularly where the channel width diminishes. Nitrogen (N<sub>2</sub>) was supplied at a standard flow rate of 100 sccm, calculated from the standard molar volume (0.0224136 m<sup>3</sup>/mol) and the mean molar mass of nitrogen (0.028 kg/mol). Boundary conditions included a prescribed flow at the inlet, atmospheric pressure at the outlet, and no-slip conditions at all solid surfaces. For precursor simulations, trimethylaluminum (TMA) was used with a diffusivity of 1×10<sup>-4</sup> m<sup>2</sup>/s and an inflow rate of 5×10<sup>-5</sup> mol/m<sup>2</sup>·s. These parameters enabled the evaluation of both velocity and concentration profiles, thereby providing insights into how the combinatorial channel design optimizes precursor distribution.

## Calculation of GI-XRD penetration depth

When a 45 kV copper anode is used, the principal X-ray lines used for diffraction are the Cu  $K\alpha$  lines ( $K\alpha_1$  and  $K\alpha_2$ ). The average wavelength for Cu  $K\alpha$  is approximately 1.5418 Å, which corresponds to an energy of 8.04 keV by using Eq. 1;

$$E = hc/\lambda \quad (\text{Eq. 1})$$

The density of ZnO, ZnAl<sub>2</sub>O<sub>4</sub>, and Al<sub>2</sub>O<sub>3</sub> has been used as 5.70, 4.59, and 3.97 g/cm<sup>3</sup> respectively. The rest of the calculations were done with a tool demonstrated in the paper of Henke *et al.* [1]

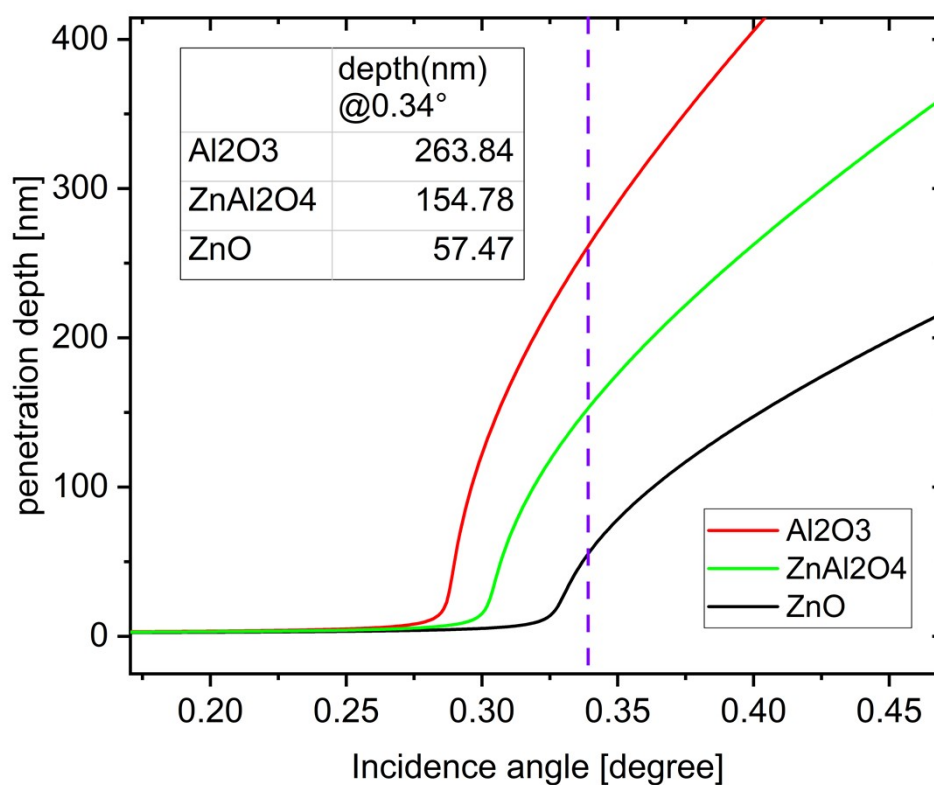


**Figure S1:** Penetration depth of the ZnO, ZnAl<sub>2</sub>O<sub>4</sub> and Al<sub>2</sub>O<sub>3</sub> materials with 0.34° incidence angle at 8040 eV energy.

## Monte Carlo Simulation of Energy-dispersive X-ray spectroscopy

Monte Carlo (MC) simulations using CASINO software were conducted to elucidate the scattering mechanisms in the R1, R2, and R3 regions, employing an 8 keV electron beam with 200,000 electrons simulated. The R1 model comprised a bulk Si substrate, a 2 nm SiO<sub>2</sub> layer, and a 40 nm ZnO film, whereas the R2 model consisted of a bulk Si substrate, a 2 nm SiO<sub>2</sub> layer, a 5 nm ZnO film, and a 3 nm Al<sub>2</sub>O<sub>3</sub> bilayer repeated eight times. The R3 model was similarly based on a bulk Si substrate with a 2 nm SiO<sub>2</sub> layer but incorporated a 5 nm ZnO film and a 5 nm Al<sub>2</sub>O<sub>3</sub> bilayer repeated eight times. The Phi-Rho-Z (PRZ) distributions were generated, where Phi ( $\phi$ ) represents the X-ray intensity, Rho ( $\rho$ ) denotes the material density, and Z corresponds to the depth within the sample, thus providing insights into the X-ray absorption characteristics of the specimen. In Figure S4, the total absorbed intensities—determined from the PRZ distributions—are presented. Elemental analysis revealed that the Zn composition was 120.7 in R1, 121.8 in R2, and 123.7 in R3, while the Si composition was 1574.4 in R1, 1480.82 in R2, and 1417.7 in R3.

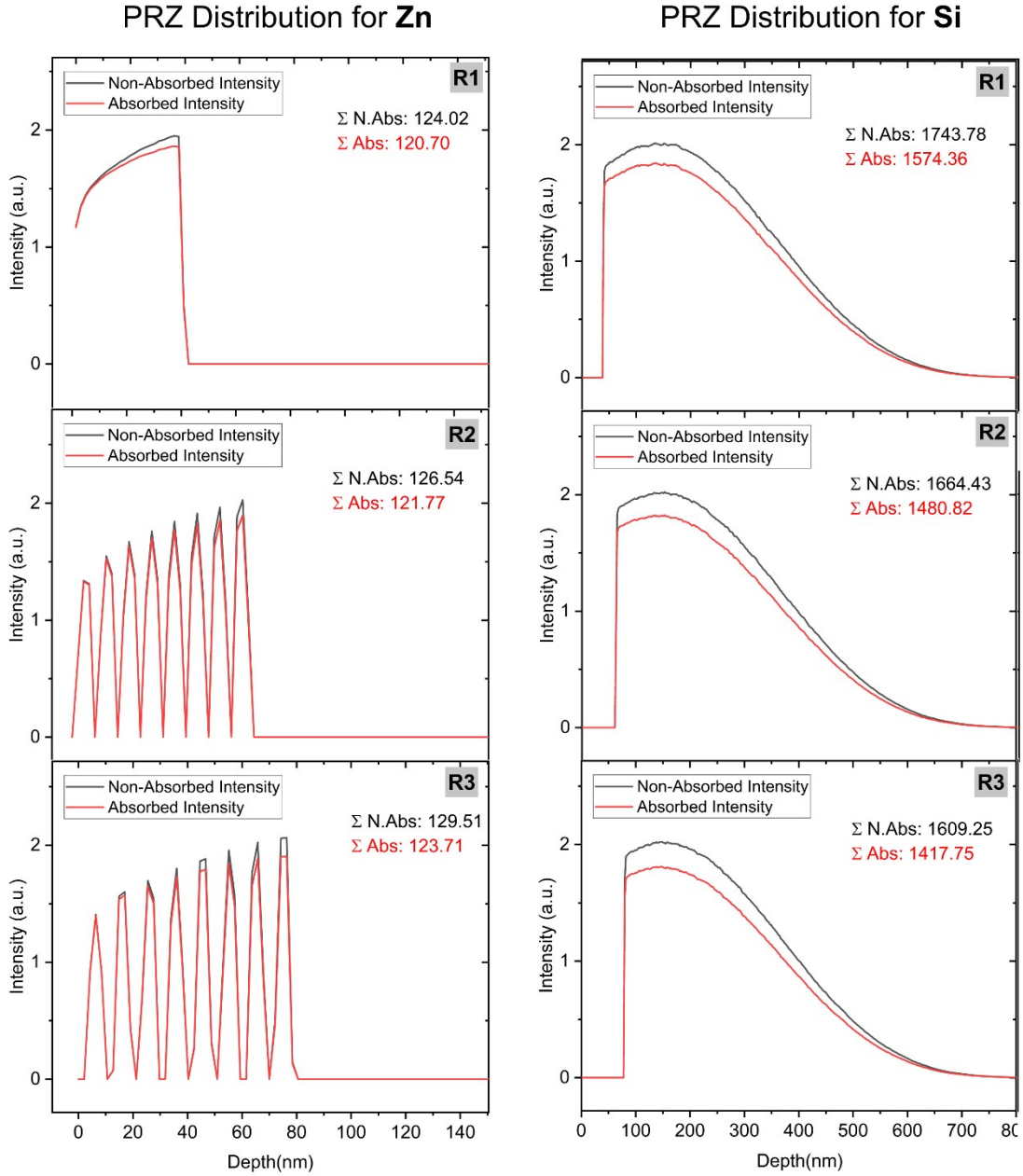


**Figure S2.** The Phi-Rho-Z (PRZ) distributions were simulated using CASINO software by modelling the R1, R2, and R3 regions of a combinatorial ZnO/Al<sub>2</sub>O<sub>3</sub> nanolaminate film.

## Surface Potential with Kelvin Probe Station

By using a reference gold (Au) sample the tip work function was calculated by using Eq. 2. The measured contact potential difference (CPD) is denoted as  $\Delta\Phi$  (in our case, 203 mV measured). The well accepted work function of Au is 5.1 eV. [2] Therefore the tip work function has been derived. Again, with the known tip work function the sample work functions were calculated.

$$\Delta\Phi = \Phi_{\text{Tip}} - \Phi_{\text{Sample}} \quad (\text{Eq. 2})$$

## X-ray Photoelectron Spectroscopy (XPS)

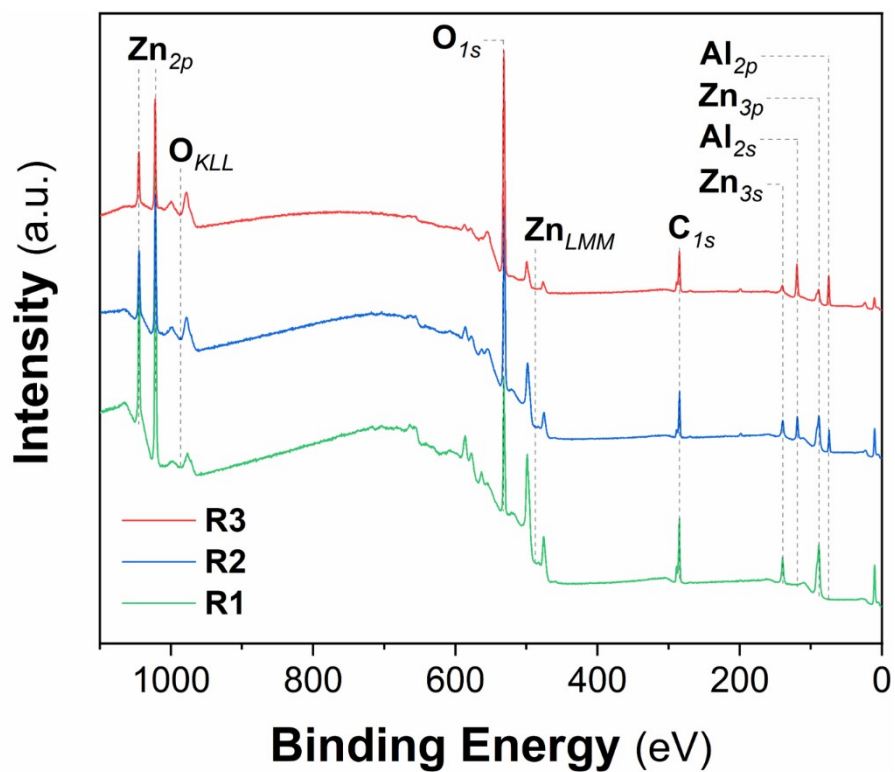


**Figure S3.** Survey spectrum of R1, R2 and R3 regions on for combinatorial ZnO/Al<sub>2</sub>O<sub>3</sub> nanolaminate films.

**Table S1.** Total atomic percentages (At.%) obtained from XPS survey spectra.

Element	At.%		
	R1	R2	R3
C	42	24	24
O	36	47	47
Zn	22	12	5
Al	-	17	24

### Quantification of oxygen from adventitious carbon and correlation with oxide-associated oxygen

According to Henderson *et al.*, the atomic percentage of oxygen originating from adventitious carbon,  $At.\% (O_{Adc})$ , can be determined from the total carbon atomic percentage,  $At.\% (C)$ , using Eq. (1), after following key assumptions and considerations detailed in Eq.3):

$$At.\% (O_{Adc}) = At.\% (C) \left[ \left[ \frac{\left(\frac{2}{3}\right)(A_B - \left(\frac{1}{2}\right)(A_D))}{100} \right] + \left[ \frac{A_C}{100} \right] + \left[ \frac{(2)(A_D)}{100} \right] + \left[ \frac{(3)(A_E)}{100} \right] \right] \quad (\text{Eq. 3})$$

where  $A_B$ ,  $A_C$ , and  $A_D$  correspond to the area percentages of the  $C^2$ ,  $C^3$ , and  $C^4$  components in the  $C_{1s}$  spectrum, respectively, while representing the area percentage of carbonate functional groups, which are not present in the current study. Then, the atomic concentration of oxygen free from adventitious carbon contributions,  $At.\% (O_{remaining})$ , was calculated from the total oxygen atomic percentage,  $At.\%(O)$ , (Eq. 4):

$$At.\%(O_{remaining}) = At.\%(O) - At.\%(O_{Adc}) \quad (\text{Eq. 4})$$

Assuming that  $At.\% (O_{remaining})$  corresponds to oxide-related oxygen, the obtained values exhibit strong agreement with the expected oxygen content in oxides,  $At.\% (O_{oxides})$ , estimated from the total atomic percentages of zinc,  $At.\%(Zn)$ , and aluminum,  $At.\%(Al)$ , under the assumption of ZnO and  $A_2O_3$ , as summarized in **Table S2**

**Table S2.** Comparison of atomic oxygen free from adventitious carbon contributions and oxygen content in oxides

Sample	At. %	
	$O_{remaining}$	$O_{oxides}^*$
R1	20	22
R2	40	38
R3	39	41

\*  $O_{oxides}$  is calculated as  $At.\%(Zn) + \frac{3}{2}At.\%(Al)$

## References

- [1] B. L. Henke, E. M. Gullikson, and J. C. Davis, "X-Ray Interactions: Photoabsorption, Scattering, Transmission, and Reflection at  $E = 50\text{--}30,000$  eV,  $Z = 1\text{--}92$ ," *At. Data Nucl. Data Tables*, vol. 54, no. 2, pp. 181–342, Jul. 1993, doi: 10.1006/adnd.1993.1013.
- [2] J. S. Kim *et al.*, "Kelvin probe and ultraviolet photoemission measurements of indium tin oxide work function: a comparison," *Synth. Met.*, vol. 111–112, pp. 311–314, Jun. 2000, doi: 10.1016/S0379-6779(99)00354-9.